J. Neural Eng. **7** (2010) 016009 (16pp) doi:10.1088/1741-2560/7/1/016009

The causal relationship between subcortical local field potential oscillations and Parkinsonian resting tremor

Peter Tass[1,2], Dmitry Smirnov[3,4], Anatoly Karavaev[4], Utako Barnikol[1,2], Thomas Barnikol[1,2], Ilya Adamchic[1], Christian Hauptmann[1], Norbert Pawelcyzk[1], Mohammad Maarouf[2], Volker Sturm[2], Hans-Joachim Freund[1,2] and Boris Bezruchko[3,4]

[1] Institute of Neuroscience and Medicine—Neuromodulation (INM-7) and Virtual Institute of Neuromodulation, Research Center Jülich, D-52425 Jülich, Germany
[2] Department of Stereotaxic and Functional Neurosurgery, University of Cologne, 50924 Cologne, Germany
[3] Saratov Branch of V A Kotel'nikov Institute of Radio Engineering and Electronics, Russian Academy of Sciences, 38 Zelyonaya Str., 410019 Saratov, Russia
[4] Department of Nano- and BioMedical Technologies, Saratov State University, 83 Astrakhanskaya Str., 410012 Saratov, Russia

Received 30 September 2009
Accepted for publication 23 December 2009
Published 19 January 2010
Online at stacks.iop.org/JNE/7/016009

Abstract
To study the dynamical mechanism which generates Parkinsonian resting tremor, we apply coupling directionality analysis to local field potentials (LFP) and accelerometer signals recorded in an ensemble of 48 tremor epochs in four Parkinsonian patients with depth electrodes implanted in the ventro-intermediate nucleus of the thalamus (VIM) or the subthalmic nucleus (STN). Apart from the traditional linear Granger causality method we use two nonlinear techniques: phase dynamics modelling and nonlinear Granger causality. We detect a bidirectional coupling between the subcortical (VIM or STN) oscillation and the tremor, in the theta range (around 5 Hz) as well as broadband (>2 Hz). In particular, we show that the theta band LFP oscillations definitely play an efferent role in tremor generation, while beta band LFP oscillations might additionally contribute. The brain→tremor driving is a complex, nonlinear mechanism, which is reliably detected with the two nonlinear techniques only. In contrast, the tremor→brain driving is detected with any of the techniques including the linear one, though the latter is less sensitive. The phase dynamics modelling (applied to theta band oscillations) consistently reveals a long delay in the order of 1–2 mean tremor periods for the brain→tremor driving and a small delay, compatible with the neural transmission time, for the proprioceptive feedback. Granger causality estimation (applied to broadband signals) does not provide reliable estimates of the delay times, but is even more sensitive to detect the brain→tremor influence than the phase dynamics modelling.

1. Introduction

Parkinson's disease (PD) in humans is a movement disorder which covers a broad spectrum of symptoms, ranging from predominant resting tremor (t-subtype) to pronounced akinesia (inability to initiate and perform movements) and rigidity (AR-subtype) [1]. The pathophysiology of Parkinsonian resting tremor still remains rather unclear [2–8]. The frequency of classical resting tremor lies between 4 and 7 Hz [9, 10]; only in early stages it may be as high as up to 9 Hz [11].

Resting tremor is centrally generated, whereas reflexes play only a marginal role for the generation of Parkinsonian resting tremor (for review, see [5]). For instance, removal of the dorsal roots in a PD patient did not abolish tremor and

only led to a reduction of the tremor amplitude and a slight change of the tremor frequency [12]. In contrast, lesions within the motor cortex, the internal capsule [13, 14] or within the thalamus or the zona incerta [14–16] may stop resting tremor. In a given patient the frequencies of tremor are often remarkably similar in different muscles [17]. In fact, tremor activity in muscles of the same part of the body (e.g. arm, leg or head) is largely coherent, whereas tremor in muscles from different extremities and, in particular, different sides is almost never coherent [18, 19]. It has been concluded that different central oscillators generate resting tremor in different extremities, accordingly [19]. It has been proposed that these independent central oscillators are most likely located in the basal ganglia loop [20].

Deep brain stimulation procedures enable intraoperative micro-/macrorecordings and postoperative macrorecordings in externalized patients (i.e. patients with implanted depth electrodes that are connected to external measurement devices) (for review see [5, 7]). Local field potentials (LFPs) can be recorded via macro- as well as microrecordings [7]. LFP recordings assess neuronal activity at a collective level [7] and, hence, provide relevant information for the analysis of synchronization processes. Pathological basal ganglia LFP activity is mainly subdivided into two major bands, <8 Hz and 8–30 Hz, where the 8–30 Hz band has further been subdivided into a 8–13 Hz and a 14–30 Hz ('beta') band [7]. Beta band activity in subthalamic nucleus (STN) and globus pallidus interni (GPi) is a prominent characteristic of basal ganglia LFP and inversely correlates with antiparkinsonian medication [21–24]. A levodopa induced decrease of beta band LFP oscillations positively correlates with an improvement of akinesia and rigidity, but not with a decrease of tremor [25]. In contrast, theta oscillations (in the tremor frequency band 3–8 Hz) are a less distinct feature of basal ganglia LFP [7], although tremor cell activity can be recorded with microelectrodes in PD patients from thalamus [26–29], pallidum [30, 31] and STN [32–36]. The discrepancy between LFP oscillations in the different frequency bands is reflected by the relationship between single unit discharges and their spike train background oscillations (representing the synchronized neuronal activity in the local vicinity of the neuron) [37]. Neurons in a high-frequency band (8–20 Hz) oscillated during longer periods and coherently with their background activity. In contrast, oscillatory neuronal activity in the tremor frequency band (3–7 Hz) occurred episodically, and only half of the single unit oscillations in the tremor frequency band were coherent with their background activity. By the same token, neurons firing at the tremor frequency have variable mutual phase relationships [38, 39]. LFP oscillations are not strictly correlated with Parkinsonian tremor [8]. However, significant tremor-associated coherence at single and/or double tremor frequencies between tremor EMGs and STN LFPs has been detected in PD patients [40, 41]. In fact, up to now there is no convincing evidence to support the hypothesis that the tremor is driven by LFP oscillations in the basal ganglia [6, 8].

To uncover the causal interdependence between LFP oscillations and tremor, it is not sufficient to study temporal correlation and/or coherence. Rather, the directionality of coupling has to be detected. A number of sophisticated, especially nonlinear techniques for the detection of directionality of couplings [42–59] have been developed and applied to different scientific fields, including geophysics [60–62], cardiology [63–66, 60] and neurophysiology [67, 68, 59, 50, 56]. We here study the causal interrelationship between LFP oscillations in the tremor frequency band in STN or VIM and Parkinsonian resting tremor. To this end, we apply a phase dynamics modelling technique [52, 53] as well as linear and nonlinear Granger causality analysis [57, 58, 69] to LFP and accelerometer signals in four Parkinsonian patients with resting tremor. We use different methods for the directionality analysis, since highly regular tremor epochs (with stable tremor frequency) alternate with less regular epochs (with variable frequency). According to theoretical studies, for the highly regular epochs the phase dynamics approach should be particularly appropriate [70], whereas for the less regular epochs Granger causality may be superior [71].

To the best of our knowledge, this is the first case where the two nonlinear techniques (phase dynamics modelling and nonlinear Granger causality) are applied to biomedical data jointly. In a short communication [72] we have presented a preliminary version of our analysis, with a smaller amount of tremor epochs, with only three patients and using only the phase modelling technique.

2. Materials and methods

2.1. Data description

We simultaneously recorded the LFP of the STN (patients 1, 3 and 4) or the VIM (patient 2) of the thalamus and the accelerometer measuring the hand tremor from four PD patients with predominant resting tremor (figure 1). Recordings were performed during or after implantation of the deep brain stimulation (DBS) electrode.

Patient 1: in this patient the tremor of the left arm was more pronounced than on the right side. Intraoperative recording from the right STN was performed with the ISIS MER system (Inomed, Teningen, Germany). *Patient 2:* unilateral tremor of the right arm. Intraoperative recording from the left VIM with the ISIS MER system. The latter is a 'Ben's gun' multi-electrode for acute basal ganglia recordings during stereotaxic operations [73], i.e. an array consisting of four outer electrodes separated by 2 mm from a central one. In patients 1 and 2 recordings were performed via the central electrode against the remote reference of the ISIS MER system. In patients 1 and 2 the results of the coupling directionality analysis were quite similar for the outer electrodes. Accordingly, we here present only the results for the central electrode.

Patient 3: bilateral tremor of both arms. Postoperative recording was performed from externalized DBS lead 3387 (Medtronic, Minneapolis) in the left STN. *Patient 4:* bilateral tremor of both arms. Postoperative recording from externalized DBS lead 3387 (Medtronic, Minneapolis) in left

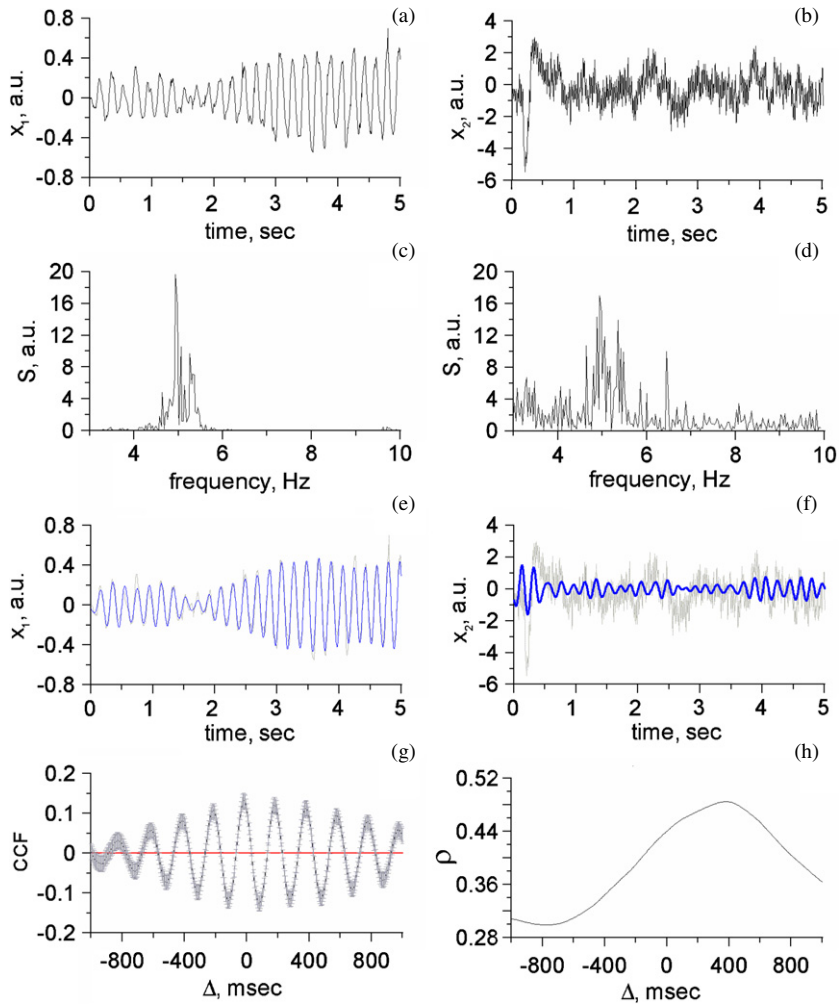

Figure 1. A spontaneous epoch of Parkinsonian resting tremor in patient 1. (a) Accelerometer signal, at the beginning of a 36 s epoch. (b) Simultaneously recorded LFP signal. (c), (d) Power spectra of accelerometer and LFP signals. (e), (f) Magnified segments of original (grey lines) and band-pass filtered (blue lines, frequency band 3–7 Hz) signals. (g) CCF between accelerometer and LFP signals with 95% confidence bands estimated with Bartlett's formula. (h) Phase synchronization index for the phases defined in the frequency band 3–7 Hz.

STN. In patients 3 and 4 the LFP was measured between tip macro-contact (contact 0, located in the target) and uppermost contact (contact 3, used as reference). In patients 3 and 4 we obtained very similar results for the coupling directionality for the two other contact pairs 1–3 and 2–3. Hence, in this paper, we only present the results for the contact pair 0–3.

Proper electrode placement was confirmed by effective high-frequency macro-stimulations, intraoperative x-ray controls [74], postoperative CT scans and intraoperative micro-recordings (in patients 1 and 2). Patients 1, 3 and 4 had a bilateral tremor, and patient 2 a unilateral tremor. The study was approved by the local ethical committee. Patients gave their written consent. In patients 1 and 2 intraoperative recordings were performed after overnight withdrawal of antiparkinsonian medication (OFF medication). In contrast, in patients 3 and 4 recordings were performed on the third postoperative day ON medication, respectively.

Accelerometer and LFP signals are denoted further as $x_1(t)$ and $x_2(t)$, $t = n\Delta t, n = 1, 2, \ldots$, and the sampling interval is $\Delta t = 5$ ms.

2.2. Coupling directionality estimation with Granger causality

A traditional tool to detect the presence of coupling between two processes is the estimation of the cross-correlation function (CCF). However, it is not straightforward to extract the 'directionality' characteristics from it. To get the estimates of the coupling strengths in different directions, we used the technique based on the construction of univariate and bivariate predictors [57, 58, 69]. If the accuracy of prediction of the x_j-dynamics can be improved by additionally taking into account the x_k-dynamics ($k \neq j$), as opposed to a univariate model, the presence of the influence $k \to j$ can be inferred.

The idea has been introduced in [69] in terms of linear models and recently it has started to be used in a nonlinear setting [57, 58]. We implemented it as follows. First, we normalized the observed time series to zero mean and unit variance for convenience. Then, we constructed univariate autoregressive models in the form:

$$\begin{aligned} x_1(t_n) &= f_1(x_1(t_{n-1}), \ldots, x_1(t_{n-d_1}), a_1) + \varepsilon_1(t_n), \\ x_2(t_n) &= f_2(x_2(t_{n-1}), \ldots, x_2(t_{n-d_2}), a_2) + \varepsilon_2(t_n), \end{aligned} \quad (1)$$

where f_j are algebraic polynomials of some orders K_j ($j = 1, 2$), a_j are vectors of their coefficients to be estimated from data, ε_j are delta-correlated Gaussian noises and d_j are the dimensions (orders) of the models. For specified values of d_j and K_j, the coefficient estimates $\hat{a}_j$ were found via the least-squares routine (LSR), i.e. by minimization of the mean-squared prediction errors. The achieved minimal value of the mean-squared prediction error for the signal x_j is given by $\sigma_j^2 = \frac{1}{N-d_j-P_j}\sum_{n=d_j+1}^{N}(x_j(t_n) - f_j(x_j(t_{n-1}), \ldots, x_j(t_{n-d_j}), \hat{a}_j))^2$ where P_j is the number of estimated coefficients in the jth equation. The quantity σ_j^2 represents an unbiased estimator of the variance of the noise ε_j. Next, we constructed bivariate models in the form:

$$\begin{aligned} x_1(t_n) &= g_1(x_1(t_{n-1}), \ldots, x_1(t_{n-d_1}), \\ &\quad x_2(t_{n-1} - \Delta_1), \ldots, x_2(t_{n-d_{\mathrm{add},1}} - \Delta_1), b_1) + \eta_1(t_n), \\ x_2(t_n) &= g_2(x_2(t_{n-1}), \ldots, x_2(t_{n-d_2}), \\ &\quad x_1(t_{n-1} - \Delta_2), \ldots, x_1(t_{n-d_{\mathrm{add},2}} - \Delta_2), b_2) + \eta_2(t_n), \end{aligned} \tag{2}$$

where g_j are algebraic polynomials of the orders K_j, $d_{\mathrm{add},j}$ are the numbers of the added values from the other signal (i.e. the characteristics of the 'coupling inertia' or 'response time'), Δ_j are trial time delays and η_j are Delta-correlated Gaussian noises. Analogously, for specified values of $d_{\mathrm{add},j}$ and Δ_j, minimal mean squared prediction errors are given by $\sigma_{k\to j}^2 = \frac{1}{N-\max\{d_j, d_{\mathrm{add},j}+\Delta_j/\Delta t\}-P_{k\to j}}\sum_{n=\max\{d_j, d_{\mathrm{add},j}+\Delta_j/\Delta t\}+1}^{N}(x_j(t_n) - g_j(x_j(t_{n-1}), \ldots, x_j(t_{n-d_j}), x_k(t_{n-1} - \Delta_j), \ldots, x_k(t_{n-d_{\mathrm{add},j}} - \Delta_j), \hat{b}_j))^2$, where $P_{k\to j}$ is the number of model coefficients in the jth equation.

Prediction improvement (PI) of the x_j-dynamics achieved by taking into account the x_k dynamics was quantified as $PI_{k\to j} = \sigma_j^2 - \sigma_{k\to j}^2$. Traditionally, such coupling characteristics are estimated for linear models ($K_j = 1$) with sufficiently high d_j and $d_{\mathrm{add},j}$, e.g. such that d_j data points cover one or several oscillation periods [69, 75, 76]. To take into account a possible nonlinearity in the dynamics and coupling, one has to confine oneself to relatively low values of d_j, $d_{\mathrm{add},j}$ and K_j. We varied d_j, $d_{\mathrm{add},j}$ for $K_j = 1$ within a wide range from 1 to 100 and for $K_j > 1$ within a narrower range from 1 to 10, having on average about 50 data points per basic tremor oscillation period. The value of Δ_j is changed within a range from 0 to 1000 ms and the point of maximum (i.e. such Δ_j^* that $PI_{k\to j}(\Delta_j^*) = \max_{0\leqslant\Delta_j\leqslant 1\mathrm{s}} PI_{k\to j}(\Delta_j)$) is taken as an estimate of the time delay in the $k \to j$ influence.

To avoid an extensive in-sample optimization, we chose reasonable values of d_j and $d_{\mathrm{add},j}$ for $K_j = 1$ by analyzing four randomly selected spontaneous tremor epochs from different patients. For this, the value of d_j at fixed K_j was selected approximately at the saturation point of the curves $\sigma_j^2(d_j)$. We tried different values of K_j and selected that one which provided the greatest prediction improvement. It was achieved at $K_j = 3$. Different small values of $d_{\mathrm{add},j}$ led to similar results of the coupling estimation. In particular, an appropriate choice of parameters seems to be $d_j = 3$ and $d_{\mathrm{add},j} = 1$. Thus, all the results of nonlinear Granger causality are presented below only for $d_j = 3$, $d_{\mathrm{add},j} = 1$ and $K_j = 3$. Typical results for $K_j = 1$ with the corresponding reasonable values of $d_j = 50$ and $d_{\mathrm{add},j} = 10$ are shown for comparison.

A pointwise statistical significance level for the conclusion '$PI_{k\to j}(\Delta_j) > 0$' at a specific Δ_j can be obtained analytically via the so-called Granger and Sargent test (F-test). However, we selected a maximal $PI_{k\to j}$ from the set $PI_{k\to j}(\Delta_j)$ for different Δ_j. Thus, it was difficult to assess analytically the total significance level for the conclusion 'the influence $k \to j$ is present' due to the necessity of a multiple test correction. Therefore, we assessed the statistical significance by surrogate data tests. To this end, we compared the value of $\max_{0\leqslant\Delta_j\leqslant 1\mathrm{s}} PI_{k\to j}(\Delta_j)$ for the observed data with the 0.95-quantile $PI_{k\to j}^*$ of the distribution of such a quantity obtained from an ensemble of AAFT (amplitude adjusted Fourier transform) surrogates [77]. These surrogates correspond to the null hypothesis of uncoupled linear autoregressive processes passed through a static monotonic transformation. Thus, for each tremor epoch we can reject the null hypothesis at the total significance level of 0.05.

We applied the linear and nonlinear Granger causality analysis to broadband LFP signals and broadband accelerometer signals. Prior to the Granger analysis the only preprocessing was to remove low-frequency trends (below 2 Hz) and power line artefacts in LFP as well as accelerometer signals with Fourier transform-based rectangular filters. LFP oscillations at frequencies below 2 Hz might be due to brain pulsations (i.e. mechanical brain oscillations that are caused by blood pulsations and are, hence, synchronized to the heart beat) which may induce modulations of the electrical potentials at the electrode–brain interface [78].

2.3. Coupling directionality estimation with phase dynamics modelling

CCF is applied to the entire signals (comprising amplitudes and phases). In contrast, to detect only the phase interdependence between the signals, one uses the time-shifted phase synchronization index [79]: $\rho(\Delta) = |\langle\exp(\mathrm{j}(\phi_1(t) - \phi_2(t+\Delta)))\rangle|$, where angle brackets denote temporal averaging (a similar index was used to study phase synchronization between Parkinsonian tremor of both hands [80]). To calculate it, we performed a band-pass filtering of $x_1(t)$ and $x_2(t)$ around the tremor frequency (e.g. 3–7 Hz in figure 1(e), (f)) with a rectangular filter and applied the Hilbert transform [81] to extract the phases $\phi_1(t)$ and $\phi_2(t)$. The computed phase values over the intervals of ten basic oscillation periods at each edge of a tremor epoch were ignored in the further analysis as recommended in [82] to avoid edge effects. Our results are stable against considerable variations of the band edges and hardly change if the lower cut-off frequency lies between 2 Hz (to filter out low-frequency components of the LFP) and $f_\mathrm{T} - 1$ Hz, where f_T is the tremor frequency. The higher cut-off frequency should be between $f_\mathrm{T} + 1$ Hz and $2f_\mathrm{T} - 1$ Hz.

The directional coupling characteristics were obtained with the phase dynamics modelling technique which resembles

the Granger causality applied to the phases [52]. As a model we use coupled phase oscillators:

$$\begin{aligned}\phi_1(t+\tau)-\phi_1(t) &= F_1[\phi_1(t),\phi_2(t-\Delta_1),a_1]+\varepsilon_1(t),\\ \phi_2(t+\tau)-\phi_2(t) &= F_2[\phi_2(t),\phi_1(t-\Delta_2),a_2]+\varepsilon_2(t),\end{aligned} \quad (3)$$

where τ is a fixed time interval equal to the basic period of oscillations, $\varepsilon_j(t)$ are zero-mean noises, F_j trigonometric polynomials of the third order [52, 53], a_j are vectors of their coefficients and Δ_j are trial time delays [83]. At each Δ_j the estimates of a_j are obtained via the least-squares routine, i.e. by searching for the minimal mean squared error $\sigma_j^2(\Delta_j) = \min_{a_j}\langle\{\phi_j(t+\tau)-\phi_j(t)-F_j[\phi_j(t),\phi_k(t-\Delta_j),a_j]\}^2\rangle$. Thereby, we get the estimate $\hat{a}_j(\Delta_j)$, i.e. the model function $F_j(\phi_j,\phi_k,\hat{a}_j)$ for each Δ_j. Coupling strength and time delay estimates are found from the dependence $\hat{a}_j(\Delta_j)$ according to the following idea.

If the 'true' equations including the 'true' coefficients $a_{j,\mathrm{true}}$ were known *a priori*, then the 'strengths' $c_{k\to j}$ of the influences $k \to j$ could be defined as $c_{k\to j}^2 = \frac{1}{2\pi^2}\int_0^{2\pi}\int_0^{2\pi}(\partial F_j(\phi_j,\phi_k,a_{j,\mathrm{true}})/\partial\phi_k)^2\,\mathrm{d}\phi_1\,\mathrm{d}\phi_2$ [52, 53]. To assess the coupling strength, we compared $c_{k\to j}$ to the mean phase increment $\phi_j(t+\tau)-\phi_j(t)\approx 2\pi$ ($\tau \approx$ a mean period). For weak coupling ($c_{k\to j} \ll 2\pi$) the contribution of the coupling terms to the phase increment is much smaller than the contribution of the basic frequency term.

The estimators $\gamma_{k\to j}$ for $c_{k\to j}^2$, expressed via the estimates $\hat{a}_j$ [53], are provided with the 95% confidence bands which read $(\gamma_{k\to j}-1.6\sigma_{\gamma_{k\to j}}, \gamma_{k\to j}+1.8\sigma_{\gamma_{k\to j}})$ where the standard deviations $\sigma_{\gamma_{k\to j}}$ are calculated from the same time series. Since $\gamma_{k\to j}$ are unbiased estimates of $c_{k\to j}^2$ under mild conditions, they can be negative although $c_{k\to j}^2 \geqslant 0$. Only positive values of $\gamma_{k\to j}$ can indicate the presence of coupling. The value of $1.6\sigma_{\gamma_{k\to j}}$ is a 0.975-quantile for the distribution of the estimator $\gamma_{k\to j}$. The pointwise significance level for the conclusion $\gamma_{k\to j}(\Delta_j) > 0$ at a certain specific Δ_j is equal to 0.025. When the range of trial time delays Δ_j covers approximately five basic periods, considerations like those given in [61] and numerical tests show that the presence of the influence $k \to j$ can be inferred at a total significance level 0.05 if the following conditions are fulfilled: (i) $\gamma_{k\to j}(\Delta_j) - 1.6\sigma_{\gamma_{k\to j}}(\Delta_j) > 0$ for a range of trial time delays Δ_j covering at least half a basic period, (ii) the phase synchronization index ρ for the corresponding time delays has to be below approximately 0.5 and (iii) the time series must not be shorter than 30–50 periods [84]. More precisely, in this case we reject the null hypothesis of uncoupled phase oscillators with Gaussian white noises ϵ_j.

In addition, the location of the maximum of $\gamma_{k\to j}(\Delta_j)$ provides an estimate of the time delay. A small τ in equation (3) (e.g. $\tau = \Delta t$) would be good for an accurate time delay estimation [83]. But the analytic confidence bands for $\gamma_{k\to j}$ [53] are reliable only if the low-order polynomials used capture the phase dynamics. This may be violated for small τ (i.e. 'fast' phase dynamics) and lead to a spurious coupling detection. Here, we preferred to ensure higher reliability of the coupling detection ($\tau \approx$ a mean period) at the cost of possibly lower accuracy in the Δ_j estimation. Δ_j can also be estimated by minimizing the model error $\sigma_{k\to j}^2(\Delta_j)$ [83]. $\gamma_{k\to j}$ is proportional to a weighted sum of squared coefficients $\hat{a}_j(\Delta_j)$. An increase in the values of the coefficients $\hat{a}_j$ minimizes σ_j^2 and maximizes $\gamma_{k\to j}$. In our data maxima of $\gamma_{k\to j}(\Delta_j)$ and minima of $\sigma_j^2(\Delta_j)$ nearly coincided.

A classical field of application of the phase dynamics modelling is the analysis of pairs of oscillatory signals generated by two self-sustained oscillators (see e.g. [52, 53, 83]). However, also in the case of noise–induced oscillations the phase dynamics modelling provides reliable results [72]. Due to its dynamical properties, the subcortical (and even cortical) oscillation in Parkinsonian patients is often considered as a self-sustained oscillator (see e.g. [85, 86]). However, mediated by its central pattern generators the spinal cord is able to produce self-sustained rhythmic neural and muscular activity [87]. Accordingly, in a first approximation even the peripheral tremor might be considered as a self-sustained oscillator.

3. Results

3.1. Single epoch analysis

3.1.1. Spectral analysis. We simultaneously measured the LFP of the STN (patients 1, 3 and 4) or the VIM (patient 2) and the accelerometer signal of the hand tremor from four patients with Parkinsonian resting tremor. Patients 1 and 2 were recorded intraoperatively after overnight withdrawal of antiparkinsonian medication, whereas patients 3 and 4 were externalized and measured on the third postoperative day in an ON medication state (see section 2).

During epochs of high-amplitude resting tremor, accelerometer signals displayed a sharp peak in the power spectrum (figure 1(c)) which was typically associated with a corresponding spectral peak in the LFP recorded from the depth electrode contralateral to (i.e. at the opposite side of) the tremor (figure 1(d)) (see [10, 9, 6, 8]). Parkinsonian resting tremor is highly regular or 'phase coherent', as verified by a determination of phase diffusion intensity of the accelerometer signal. To obtain a rough estimate of the phase diffusion intensity, we determined the coefficient of variation of the instantaneous period of the accelerometer signal band-pass filtered around the tremor frequency (e.g. from 3 to 7 Hz as shown in figure 1(c)): $k = \langle T_i\rangle^{-1}\sqrt{\langle(T_i-\langle T_i\rangle)^2\rangle}$, where angular brackets denote averaging over time and T_i are the intervals between successive maxima of the signal. In the ensemble of 48 tremor epochs considered in this study, we obtained k typically in the range of 0.01–0.4, predominantly 0.05–0.1. For the highly regular tremor epochs (the smallest values of k) a very appropriate technique for the directionality analysis is the phase dynamics approach [70], whereas for less regular epochs the Granger causality may be superior [71].

3.1.2. Phase dynamics modelling. The results for the coupling between the LFP and the tremor of the contralateral hand during a single typical tremor epoch from patient 1 are shown in figure 2. We revealed a significant interdependence between the signals even with the cross-correlation function

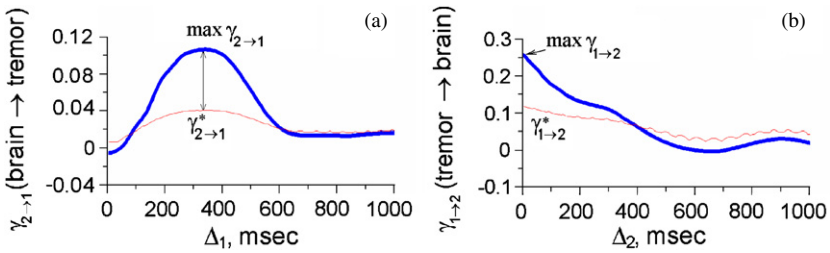

Figure 2. Phase dynamics modelling analysis of the epoch shown in figure 1. The coupling strength estimates are shown versus trial time delay (blue lines). The red lines denote the analytically estimated pointwise 0.975-quantile given by $\gamma^*_{k\to j} = 1.6\sigma_{\gamma_{k\to j}}(\Delta_j)$. (a) Estimated brain→tremor influence. (b) Estimated tremor→brain influence.

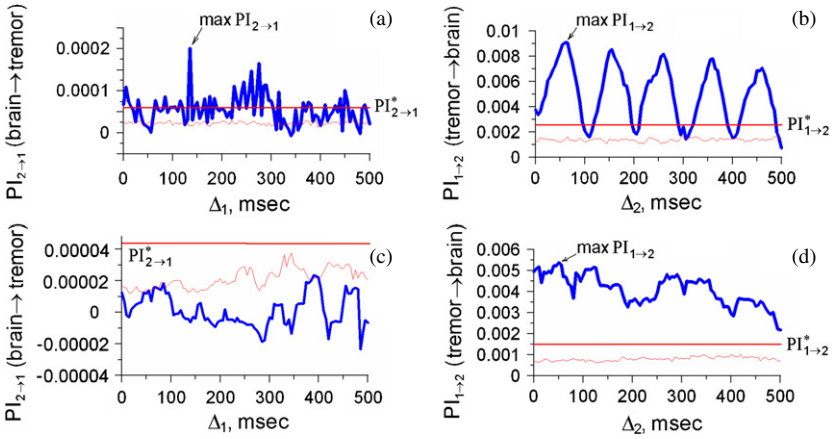

Figure 3. Granger causality estimation for the epoch shown in figure 1. Coupling strength estimates are shown versus trial time delay. The thin red lines denote the pointwise 0.95-quantile of the statistics obtained from an ensemble of 100 AAFT surrogates. The thick red lines show the 0.95-quantile of the quantity $PI^*_{k\to j} = \max_{0\leqslant\Delta_j\leqslant 1s} PI_{k\to j}(\Delta_j)$. Nonlinear Granger causality [(a), (b)]: $d_j = 3$, $d_{\mathrm{add},j} = 1$, $K_j = 3$. Linear Granger causality [(c), (d)]: $d_j = 50$, $d_{\mathrm{add},j} = 10$, $K_j = 1$. (a), (c) Estimated brain→tremor influence. (b), (d) Estimated tremor→brain influence.

(figure 1(g)). The mean phase coherence $\rho = 0.48$ at $\Delta = 385$ ms (figure 1(h)) which is not too high so that the phase dynamics modelling is applicable. LFP and accelerometer signals were both band-pass filtered around the tremor frequency prior to performing the phase dynamics modelling analysis (see also section 4). The phase dynamics modelling reveals a significant influence in both directions (figure 2). The contralateral tremor→brain influence is very pronounced and reaches its peak value at zero trial delay: $\gamma_{1\to2}(0) = 0.26$. As we conclude below, the time delay for this direction is at most several dozens of milliseconds. The brain→tremor influence is also highly significant: $\gamma_{2\to1}(335) = 0.1$. For this direction, the time delay $\Delta_1 = 335$ ms is pronounced and considerably different from zero.

The analytical pointwise 0.975-quantiles are indicated by the red lines in figure 2. The peak values of $\gamma_{k\to j}$ in figure 2 obtained from the real data are much greater. According to the above-mentioned analytical test, $\gamma_{k\to j}$ are significant at the total significance level of $p < 0.05$.

3.1.3. Granger causality. Granger causality analysis was applied to broadband LFP and accelerometer signals (see also section 4). Granger causality estimates for the same epoch of spontaneous tremor are presented in figure 3. Nonlinear Granger causality estimation (figure 3(a), (b)) gives results similar to the phase dynamics analysis in the sense that it also detects a bidirectional coupling. In contrast, linear Granger causality reveals only the 'tremor → brain' influence (figure 3(c), (d)). Such a combination of results is typical as shown below for many spontaneous tremor epochs. However, the peak values of $PI_{\mathrm{brain}\to\mathrm{tremor}}$ in figure 3(a), (b) are observed at values of the trial time delay which are different from the peaks of $\gamma_{\mathrm{brain}\to\mathrm{tremor}}$. Moreover, the time delay Δ_1 corresponding to the peak values of $PI_{\mathrm{brain}\to\mathrm{tremor}}$ considerably varies across different tremor epochs in contrast to a peak time delay for $\gamma_{\mathrm{brain}\to\mathrm{tremor}}$ which is comparatively stable (see below).

3.2. Ensemble of tremor epochs

In all patients epochs with tremor occurred intermittently. To reveal reliable coupling estimates with the phase dynamics modelling, we had to select tremor epochs of sufficient length. However, due to the nonstationarity of the data, the time series should not be too long. Tremor epochs of a length not shorter than 70 basic periods turned out to be the optimal trade-off. In contrast, the estimation results in shorter epochs strongly fluctuate, so that the shape of the curves $\gamma_{k\to j}(\Delta_j)$ may vary considerably. This can be interpreted as the effect of noise, which is reduced when longer epochs are used.

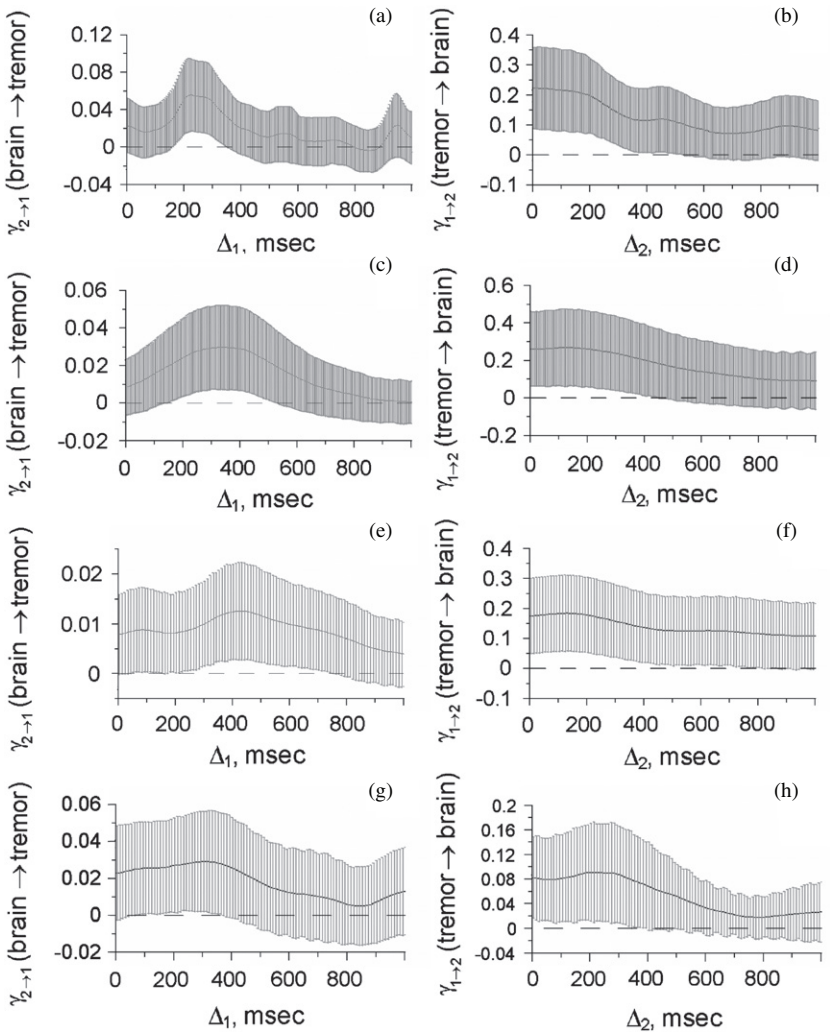

Figure 4. Coupling characteristics obtained from the phase dynamics modelling and averaged over many epochs for each patient. Error bars indicate 95% confidence intervals obtained via averaging of the analytical confidence intervals. (a), (b) Patient 1 (basic tremor frequency is 5 Hz, filter frequency band used to calculate the phases is 3–7 Hz, number of epochs is 12, duration of epochs ranges from 16.5 s to 83.5 s). (c), (d) Patient 2 (4 Hz, 2–6 Hz, 14, 17.5–45.0 s). (e), (f) Patient 3 (5 Hz, 3–7 Hz, 8, 15.0–55.0 s). (g), (h) Patient 4 (5 Hz, 3–6 Hz, 14, 20.0–60.0 s).

3.2.1. Phase dynamics modelling. Figure 1 shows one of the long epochs, consisting of 180 periods. That interval exhibits a typical directionality pattern (figure 2) reproduced for a high percentage of epochs. We observed a statistically significant brain→tremor coupling in 65% of all epochs (in 8 out of 12 epochs in patient 1, in 10 out of 14 epochs in patient 2, in 6 out of 8 epochs in patient 3 and in 7 out of 14 epochs in patient 4). Conversely, in 35% of all epochs, a significant brain→tremor influence was not detected. Furthermore, we revealed a statistically significant tremor→brain coupling in 54% of all epochs (in 8 out of 12 epochs in patient 1, in 8 out of 14 epochs in patient 2, in 4 out of 8 epochs in patient 3 and in 6 out of 14 epochs in patient 4). For every patient we averaged the directionality results across all epochs, respectively (figure 4). In this way for all four patients we obtained consistent results, confirming the coupling pattern from figure 2. We obtained a bi-directional coupling at time delays close to 0 for the contralateral tremor→brain direction and a delay of about 1–2 mean periods of the tremor (200–400 ms) for the brain→contralateral tremor direction with average values $\gamma_{2\to1} = 0.03$–0.05 and $\gamma_{1\to2} = 0.20$–0.25.

Figure 5 illustrates the combined results of the statistical significance tests for all epochs analyzed. For each epoch we show the value of $\gamma_{k\to j}$, maximized over the range of trial time delays (0–500 ms), divided by the respective pointwise 0.975-quantile $\gamma^*_{k\to j}$ (see figure 2 for an illustration). If the ratio exceeds unity, then the presence of the respective driving is inferred at the total significance level of $p < 0.05$ (it appears that the other requirements mentioned in section 2.3 are fulfilled). Figure 5 shows that significant 'brain → tremor' influence is detected in approximately 65% of epochs. Despite the strength of the opposite influence being greater, the tremor→brain influence itself is revealed in only 50% of epochs. This is because the phase dynamics of the brain signals is much more 'noisy' and, hence, prevents the confident unmasking of the 'tremor → brain' impact. Yet, the percentage of epochs exhibiting statistically significant couplings in both directions is quite high (much greater

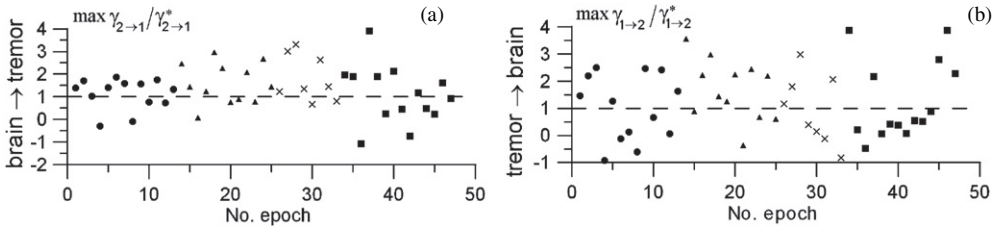

Figure 5. Phase dynamics modelling of an ensemble of tremor epochs of the four patients. The ratio of the maximal coupling strength to the analytical pointwise 0.975-quantile is shown versus the number of the epoch. Different symbols belong to the four different patients, respectively. The dashed line indicates the unity level. Ratios higher than unity correspond to a coupling detection at a total significance level of $p < 0.05$. (a) Estimated brain→tremor influence. (b) Estimated tremor→brain influence.

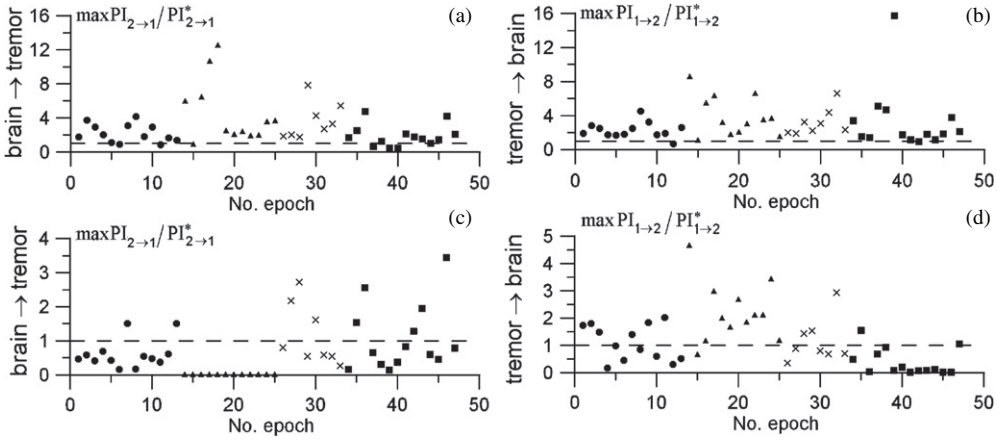

Figure 6. Granger causality estimation for an ensemble of tremor epochs of the four patients. The ratio of maximal PI to the AAFT surrogates based on 0.95-quantile $PI^*_{k\to j}$ is shown versus the number of the epoch. Different symbols correspond to the four different patients. The dashed lines indicate the unity levels. Ratios higher than unity correspond to a coupling detection at a total significance level of $p < 0.05$. Nonlinear Granger causality [(a), (b)]: $d_j = 3$, $d_{\mathrm{add},j} = 1$, $K_j = 3$. Linear Granger causality [(c), (d)]: $d_j = 50$, $d_{\mathrm{add},j} = 10$, $K_j = 1$. (a), (c) Estimated brain→tremor influence. (b), (d) Estimated tremor→brain influence.

than the 5% of random erroneous conclusions expected for uncoupled processes).

3.2.2. Granger causality. Granger causality estimation was performed for all of the above-mentioned tremor epochs. Remarkably, significant bidirectional coupling (e.g. figure 3) was detected even more often with the nonlinear Granger causality than with the phase dynamics analysis. In figure 6 we plot PIs maximized over the range of trial delays divided by the pointwise 0.95-quantile $PI^*_{k\to j}$ obtained from an ensemble of 100 AAFT-surrogate time series. If the ratio is greater than 1, we infer the presence of coupling at the pointwise significance level $p < 0.05$. Nonlinear Granger causality estimations allow us to detect 'brain → tremor' driving in 85% of epochs and the opposite coupling in 96% of epochs. In contrast, linear Granger causality can detect coupling much less reliably: 26% for the 'brain → tremor' direction and 47% for the 'tremor → brain' direction. Thus, the nonlinear techniques are much more sensitive than the linear one and both of them provide consistent results about the presence of bidirectional coupling.

However, in contrast to the phase dynamics modelling, the plots of PIs versus trial time delay exhibit peaks at different locations for different tremor epochs. Therefore, the averaged plots of PIs are not informative since they do not exhibit clear peaks (not shown). Thus, no 'stable' time delay estimate can be claimed with confidence. This result can be interpreted taking into account that the phase dynamics modelling concentrates on the specific frequency band around the tremor frequency where one could expect a unique time delay. The Granger causality estimation is applied to the original signals with only the slow component (frequencies below 2 Hz) removed. Thus, Granger causality analysis relates to a wide range of frequencies. Since one can naturally expect different time delays for different frequency bands, a clear time delay cannot be observed from such an integral analysis. Still, some signs of the time delays consistent with the phase dynamics modelling results can be seen in the histograms of figure 7. These histograms were constructed by selecting for each epoch the five largest maxima on the plot 'PI versus trial time delay' exceeding the total 0.95-quantile $PI^*_{k\to j}$ (e.g. figure 3) and considering their locations as possible time delay estimates. Thus, in total we obtained about 200 values of the time delay estimate for each of the two directions. The resulting histograms shown in figure 7 allow us to detect accumulation points of the time delays at about 0 and at about 300 ms time delays in the 'brain → tremor' direction and at 50 ms time delay in the 'tremor → brain' direction.

3.2.3. Spectral characteristics. A central aspect of our study is to clarify the efferent function of the LFP oscillations. The

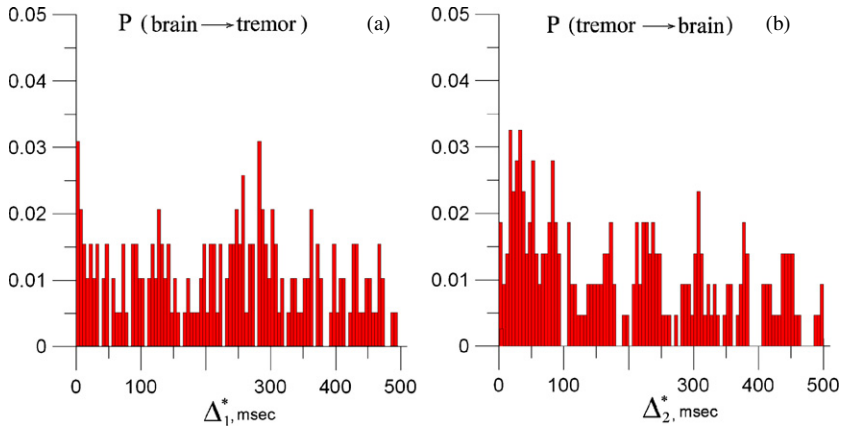

Figure 7. Histograms of the time delay estimates obtained with the nonlinear Granger causality estimation ($d_j = 3$, $d_{\mathrm{add},j} = 1$, $K_j = 3$) of all 48 tremor epochs of the four patients. (a) Brain→tremor influence. (b) Tremor→brain influence.

Table 1. Spectral characteristics of the LFP recordings for the tremor epochs where the brain→tremor influence is detected with both the phase dynamics modelling and the nonlinear Granger causality analysis. $\langle P_\theta \rangle$ denotes the mean spectral power in theta band (3–7.5 Hz) of a single tremor epoch; $\langle P_\alpha \rangle$ and $\langle P_\beta \rangle$ denote the corresponding quantities in the alpha band (8–13 Hz) and in the beta band (14–30 Hz). We present the statistical characteristics of the power ratios for the ensembles of epochs by providing mean value ± standard deviation; minimal value; maximal value.

Patient no	$\langle P_\theta \rangle / \langle P_\alpha \rangle$	$\langle P_\theta \rangle / \langle P_\beta \rangle$
1 (7 epochs)	3.1 ± 1.2; 1.9; 5.0	6.1 ± 3.1; 3.9; 12.1
2 (8 epochs)	4.5 ± 2.2; 2.3; 9.3	9.3 ± 3.9; 3.9; 16.9
3 (4 epochs)	8.0 ± 5.7; 3.7; 16.3	29.6 ± 20.7; 8.0; 56.5
4 (7 epochs)	5.9 ± 5.4; 3.1; 18.1	23.2 ± 31.2; 7.0; 91.2

phase modelling analysis revealed an efferent contribution of the theta band oscillations in tremor generation. On the other hand, the nonlinear Granger causality analysis showed the efferent influence of the broadband LFP at even higher levels of sensitivity. Hence, LFP rhythms other than theta might play a tremor generating role, too.

To assess whether oscillations at higher frequencies than theta might contribute to tremor generation, we determined the spectral LFP characteristics of the tremor epochs where the brain→tremor influence was detected with both the phase dynamics modelling and the nonlinear Granger causality analysis (table 1) and compared it with the spectral characteristics of the tremor epochs where the brain→tremor influence was detected only with the nonlinear Granger causality, but not with the phase dynamics modelling (table 2).

Apart from theta band (3–7.5 Hz) activity we observed relevant frequency components in the alpha band (8–13 Hz) and beta band (14–30 Hz), but no relevant peaks in the gamma band (> 60 Hz). Accordingly, in the epochs specified above we analyzed the mean spectral power in the theta band $\langle P_\theta \rangle$, the alpha band $\langle P_\alpha \rangle$ and the beta band $\langle P_\beta \rangle$. We computed mean, standard deviation, minimal and maximal value of the ratios $\langle P_\theta \rangle / \langle P_\alpha \rangle$ and $\langle P_\theta \rangle / \langle P_\beta \rangle$ (tables 1 and 2).

The overall leading frequency component was in the theta band (tables 1 and 2). However, in all patients we found

Table 2. Spectral characteristics of the LFP recordings for the tremor epochs where the brain→tremor influence is detected with the nonlinear Granger causality, but not with the phase dynamics modelling. Same format and notation as in table 1.

Patient no	$\langle P_\theta \rangle / \langle P_\alpha \rangle$	$\langle P_\theta \rangle / \langle P_\beta \rangle$
1 (4 epochs)	3.2 ± 0.5; 2.5; 3.7	7.2 ± 3.5; 3.6; 11.9
2 (3 epochs)	3.3 ± 2.7; 1.4; 6.4	6.0 ± 4.7; 3.1; 11.4
3 (4 epochs)	7.4 ± 3.2; 4.0; 11.8	21.1 ± 9.2; 9.0; 28.7
4 (7 epochs)	4.6 ± 2.9; 1.8; 10.7	10.5 ± 8.4; 2.9; 28.4

additional activity in the alpha and beta bands (tables 1 and 2). Beta band activity was stronger, i.e. $\langle P_\theta \rangle / \langle P_\beta \rangle$ was smaller, in patients 1 and 2, who were OFF medication, as opposed to patients 3 and 4, who were ON medication (tables 1 and 2).

In the context of tremor generation it is interesting that the LFP tends to have a stronger beta band activity in epochs where the LFP→tremor influence is detected with nonlinear Granger causality analysis only (table 2). However, the limited number of epochs does not allow for a statistically solid judgement. Nevertheless, this finding indicates that—in addition to theta band activity—beta band activity might be involved in tremor generation.

4. Discussion

Our investigation of the dynamical generation of Parkinsonian resting tremor in an ensemble of 48 tremor epochs in four PD patients revealed a bidirectional coupling between LFP oscillations in the STN (in three patients) or the VIM (one patient) and the tremor. The brain→tremor driving was reliably detected only with the nonlinear techniques, the phase dynamics modelling and the nonlinear Granger causality analysis. Both nonlinear techniques revealed similar results, but still there were differences. On the one hand, the nonlinear Granger causality estimation (with an appropriately chosen model structure) enables us to reveal this efferent driving for almost all tremor epochs of sufficient length, while the phase dynamics modelling reveals this driving in 65% of epochs. On the other hand, the phase dynamics modelling consistently reveals a delay time of 1–2 mean tremor periods (200–400 ms),

while the Granger causality does not detect the delay time reliably. However, slight signs of the time delay presence can be detected by the Granger causality estimates as well (figure 7).

4.1. Data analysis

A numerical analysis of model systems showed that the time resolution of the phase modelling technique is limited [72]. Worst case errors of the time delay estimates may be as high as half a basic period of the oscillation. This has to be taken into account for the interpretation of the time delay estimates revealed with the phase modelling technique (figure 4). Though limited in precision, our delay estimates show that the delay for the brain→tremor driving is considerably greater than that for the reverse direction. In addition, the delay estimate for the tremor→brain driving is close to zero, i.e. small compared to its worst case error. The median nerve sensory evoked potential intraoperatively recorded from DBS leads in VIM or STN in PD patients had a peak latency at 17.3 ms and 18.7 ms, respectively [88]. Hence, the neural transmission time (approx. 10–20 ms) is the candidate most likely to be the physiological correlate of the small delay estimate for the tremor→brain influence. By contrast, the long brain→tremor delay indicates a more complex mechanism compared to a simple efferent neural transmission. Accordingly, in a way our results provide a new variant of the old servo loop oscillation concept, where feedback and feedforward information are acting through direct transmission lines [89]. Rather, our findings suggest that the synchronized subcortical oscillations feed into a multistage re-entrant network, most likely comprising cortico-subcortical and spinal reflex loops (see e.g. [90, 91]).

The phase modelling analysis and the (linear and nonlinear) Granger analysis performed in this study differ in two respects.

- Amplitude dynamics versus phase dynamics: both linear and nonlinear Granger causality analysis take into account amplitudes and phases of the signals, whereas the phase modelling technique selectively studies the phase dynamics only (i.e. without consideration of the amplitude dynamics). The motivation to study the phase dynamics selectively comes from the observation that the coordination of phases and, in particular, phase synchronization has been shown to be a fundamental mechanism for motor control under healthy conditions in both animals and humans [92–94, 86]. Furthermore, a magnetoencephalography study revealed phase synchronization between brain activity and muscular activity [85].
- Narrow-band versus broad-band signals: the phase modelling technique requires that the phases of the signals under study are determined in a well-defined way. Consequently, one has to perform a band-pass filtering in order to extract the signal belonging to a prominent peak in the frequency spectrum (for review see [82]). In contrast, we here apply the (linear and nonlinear) Granger causality analysis to broadband signals. To this end, in both LFP and accelerometer signals we only removed low-frequency trends (below 2 Hz) and power line artefacts. The motivation to go for a broadband analysis is twofold. (i) In PD patients coherence between single units and tremor has predominantly been found in the tremor frequency range, but, nevertheless, also at frequencies in the beta band (see below) [35]. In fact, it is not yet resolved to what extent beta band activity contributes to tremor (see, e.g., [39, 22, 95, 96]). As demonstrated in PD patients, different LFP frequency bands from STN may have different bidirectional interaction with mesial and lateral cortical areas (see below) [91]. However, this does not imply that the different frequency bands, especially theta and beta bands, are completely separate from a dynamical point of view and fulfill a superposition assumption. We wanted to avoid such a superposition assumption since it is not proven. Moreover, from the standpoint of oscillator theory, in complex systems such a superposition assumption can certainly not be considered as generic. (ii) Applying the Granger causality analysis to band-pass filtered signals is per se not trivial. For instance, after band-pass filtering, a signal x_j may get rather smooth and, hence, allow for a precise one-step-ahead prediction that may hardly be topped by additionally taking into account signal x_k ($k \neq j$). Accordingly, the band-pass filtering may result in an artificially high univariate prediction baseline which may hinder reliable and sensitive detection of directional coupling.

The sensitivity of the broadband Granger analysis is better than that of the theta band phase modelling technique. Accordingly, to assess the possible impact of frequency bands other than theta, we analyzed the spectral composition of the LFPs. Apart from theta band activity we also found relevant alpha and beta band components (tables 1 and 2). In contrast, in the selected resting epochs (without active and passive movements) we did not find any relevant peaks in the gamma frequency band (>60 Hz). This is accordance with the notion that gamma band activity is considered to be prokinetic in nature [6] and emerges, e.g., before voluntary movements [97]. Interestingly, there is a tendency for tremor epochs for which the LFP→tremor driving is detected with the nonlinear Granger analysis only (and not with the phase modelling technique) to display stronger beta band activity (tables 1 and 2). However, due to the limited number of epochs a statistically solid judgment cannot be derived. Nevertheless, this finding indicates that—apart from theta band activity—beta band activity might additionally be involved in tremor generation. Such an efferent role of beta oscillations is also compatible with (but not proven by) observations in PD patients showing that 52.4% of the STN single units are coherent with tremor in the theta band, whereas 6.9% of the STN single units are coherent with tremor in the beta band (15–30 Hz) [35]. Accordingly, beta band LFP oscillations might contribute to tremor generation, without playing a dominant role. Such a notion is compatible with the observation that a levodopa-induced decrease of beta band LFP activity causes an improvement of akinesia and rigidity, but not a decrease of tremor [25].

The phase modelling technique applied to narrow-band (theta) oscillations reveals consistent estimates of the delay times (figure 4). In contrast, the delay estimation with the nonlinear Granger causality analysis applied to broadband signals is not reliable (figure 7). We may speculate on two possible reasons behind the poor delay estimation obtained with the nonlinear Granger analysis. On the one hand, this may be due to features inherent to the method. On the other hand, this may reflect the complex pathophysiology, in that neuronal activity in different frequency bands may differentially feed into different loops with different delays (see e.g. [90, 91]), which might hamper a precise delay estimation.

LFP signals recorded from STN in PD patients led EEG signals recorded from sensors over the mesial and lateral cortex [91]. The pattern of the bidirectional interactions between the mesial cortex and STN on the one hand and the lateral cortex and STN on the other hand does not significantly differ in drug ON versus drug OFF states in both the sub-beta band (3–13 Hz) and beta band (14–35 Hz). Only in the gamma band (65–90 Hz) the bidirectional cortex/STN interactions increased in the drug ON condition. Concerning medication ON/OFF-induced changes, it should be noted that in our study in patients 1 and 2 intraoperative recordings were performed OFF medication, whereas in patients 3 and 4 recordings were performed on the third postoperative day ON medication. In accordance with previous studies [25], the beta band activity in the patients OFF medication was stronger (relative to the theta band activity) than that in the ON medication state. The target in patient 2 was the VIM, whereas in patients 1, 3 and 4 leads were implanted in the STN. Accordingly, our findings indicate that the bidirectional driving between STN and tremor is present both ON and OFF drugs.

The tremor→brain influence could be detected with any of the techniques used in this study, even with the linear Granger analysis. Remarkably, the brain→tremor driving can only be reliably detected with the nonlinear data analysis methods, the phase modelling technique and the nonlinear Granger analysis. In accordance with our results a study on the relationship between tremor and electroencephalographic (EEG) recordings with partial directed coherence (a linear data analysis technique) revealed only a proprioceptive impact of the electromyographic (EMG) signal on the EEG signals (channels C4 and PZA, both displaying strong correlation with the EMG at the tremor frequency), but no brain→tremor driving [75].

In a numerical study on coupled neuron models the phase modelling approach has been compared to the partial directed coherence [71]. As yet, the only comparative study on biomedical signals is an investigation of epileptic EEG recordings performed with the phase dynamics modelling technique and the state space nearest-neighbour characteristics [49].

4.2. Pathophysiology

In PD patients with resting tremor Wang and co-workers studied the causal interdependence between EMG signals and corresponding LFP signals recorded through depth electrodes implanted in the STN [98]. The directionality analysis was performed with linear adaptive Granger autoregressive modelling, however, without testing for statistical significance. During persistent tremor they revealed a strong proprioceptive (tremor→brain) influence, whereas during episodes of transient tremor the interrelationship was bidirectional or alternatively varied [98]. The validity of this study is limited since no confidence intervals or significance levels were computed and, hence, the statistical relevance of the computed values remains an open issue. Furthermore, related to this aspect, it remains unclear how to distinguish between fluctuations of estimates and a reliable detection of coupling characteristics when performing the analysis in a running window of only 3 s length.

In one PD patient Florin and co-workers [99] applied linear Granger causality to the tremor EMG and the LFP recorded with a macroelectrode placed in the STN. They reported that for three pathways the LFP was purely efferent, and for one pathway there was a bidirectional relationship between LFP and tremor. It is difficult to appreciate these findings appropriately since details and parameters of the analysis were not reported.

A number of studies have been devoted to tremor-related single unit activity in human PD patients. Single unit activity in the ventrolateral thalamus has been intensively studied during stereotactic surgery [26–29, 100–104]. The nucleus ventralis caudalis (Vc) mainly contains sensory cells (responding to sensory stimulation). The motor thalamus, located anterior to the Vc, contains the ventral intermediate nucleus (VIM) and the ventral oral posterior nucleus (VOP). The pallido-thalamic fibres terminate in the VOP, whereas the cerebello-thalamic fibres terminate in the VIM [105, 106]. VIM and VOP contain voluntary cells (active during voluntary movements only) and combined cells (active during movement and responding to somatosensory stimulation). Tremor cells have been found among the three cell types [28, 29]. 50% of the combined cells, 22% of the voluntary cells and 53% of the sensory cells were tremor cells [103]. Combined and voluntary cells typically have a phase advance relative to the peripheral tremor burst, whereas the sensory cells typically exhibit a phase lag [28, 29]. Accordingly, it has been suggested that the combined and voluntary cells cause the tremor [28, 29]. However, in general one has to be highly cautious when identifying phase lags with causal relationships.

The results of a detailed analysis of the inter-spike intervals within the tremor-related thalamic bursts were not consistent with two specific tremor generation hypotheses [104]. (i) The thalamus-GPi-pacemaker hypothesis [107] posits a central generator consisting of overactive neurons in the internal segment of the globus pallidus inhibiting/hyperpolarizing the thalamic neurons [107], (ii) the oscillation of an unstable long loop reflex arc transmitting activity from muscle stretch receptors to thalamus, motor cortex, and back to the muscles [108, 109].

Microrecordings have revealed tremor-related 3–7 Hz bursting of oscillatory single-cell activity in STN of human PD patients [33, 32, 110, 111]. In a study devoted to the spectral coherence between spike activity of STN neurons and

tremor activity, significant coherence was found in 52.4% of the neurons at the tremor frequency and in 6.9% of the neurons in the beta band [35]. The tremor-coherent STN spiking activity was extensively found all over the STN, preferentially in its dorsal parts (70.8–88.9%) as opposed to its ventral parts (25.0–48.0%) [35]. These microrecording studies demonstrate that the tremor rhythm can be found in the STN. However, based on these findings it cannot be judged whether the tremor rhythm in the STN is afferent, i.e. driven by a proprioceptive feedback through the indirect pathway via the basal ganglia or through a direct projection from the cortex, or whether the tremor rhythm in the STN is efferent, i.e. generated within the basal ganglia and driving the tremor (for review see [5]).

There are two hypotheses on mechanisms underlying Parkinsonian symptoms involving abnormal synchronized STN activity.

- The STN-GPe-pacemaker hypothesis [112]: in an *in vitro* model comprising cortex, striatum, STN and external pallidum (GPe), it has been shown that STN and GPe may constitute a pacemaker at frequencies between 0.4 Hz and 1.8 Hz [112]. To what extent this animal *in vitro* model applies to human PD remains unclear. On the one hand, the frequencies are below the typical frequencies encountered in PD, which might be due to the fact that the *in vitro* model is a reduced model compared to the situation in an entire brain, which additionally contains loops and projection systems (e.g., cortico-STN and cerebello-thalamo-cortical projections) that may modulate the frequency of basal ganglia rhythms. On the other hand, oscillatory single unit activity has only infrequently been found in the GPe of human PD patients [113].
- The loss of segregation hypothesis [114, 115, 20, 116, 8] is based on the *in vivo* MPTP primate model of PD [8, 20, 115]. In the MPTP monkey it has been shown that neurons in different regions of the basal ganglia fire coherently, whereas in the healthy monkey they fire in an uncorrelated manner [8, 115]. Neuronal oscillatory activity is synchronized not only within single basal ganglia nuclei, but also between different nuclei [21, 95]. Not a focal generator, but the whole basal ganglia network generates neural oscillations and synchronization [8]. The parallel basal ganglia loops lose their ability to separately process information and join into a widely distributed coherent action. However, as yet only akinesia and rigidity have been tightly attributed to the synchronous LFP oscillations in the basal ganglia network [7, 8]. Since Parkinsonian tremor is not strictly correlated with the LFP oscillations, it has been proposed that the tremor is not (directly) generated by the synchronized basal ganglia oscillations, but might, e.g., emerge as a downstream compensatory mechanism [8].

Our results show that there is a bidirectional coupling between the tremor and LFP oscillations (in the tremor frequency range as well as broadband) in both STN and VIM. Concerning tremor generation, the theta band LFP oscillations definitely play an efferent role, while the beta band LFP oscillations might additionally contribute. Our findings support the loss of segregation hypothesis. In fact, in some sense our results round the loss of generation hypothesis out by demonstrating that not only akinesia and rigidity [7, 8], but also tremor is generated by basal ganglia and thalamic oscillations. For this study we have used different data analysis methods that are in several respects complementary. Their results confirm each other to a significant extent.

LFP oscillations measured by depth electrodes are generated by the synchronized current changes in a large number of neurons (for review see [7]). Our results show that the LFP oscillations in STN and VIM drive the tremor. Accordingly, this supports an approach which aims at specifically counteracting tremor by desynchronizing the abnormally synchronized subcortical populations of oscillatory neurons [117], e.g. with coordinated reset stimulation [118]. The classical targets STN and VIM may serve as candidate target areas for desynchronizing deep brain stimulation. By contrast, up to now permanent deep brain stimulation at frequencies greater than 100 Hz is applied to suppress Parkinsonian symptoms [119]. This type of stimulation strongly alters the affected neuronal population, e.g. by completely blocking the neuronal firing [120, 121].

5. Conclusions

We reveal a bidirectional interaction between the tremor and the LFP oscillations in VIM or STN in the tremor frequency range as well as in a broad frequency band (> 2 Hz). Intriguingly, the tremor is significantly influenced by LFP oscillations in STN and VIM. This efferent (brain→tremor) influence is a complex, nonlinear mechanism, which can only be reliably detected with the two nonlinear techniques. By contrast, the afferent (tremor→brain) driving is detected with any of the techniques including the linear Granger analysis. However, the latter is by far the least sensitive method. With the phase dynamics modelling (applied to the tremor frequency band), we consistently reveal a long delay in the order of 1–2 mean tremor periods for the efferent driving and a small delay that is compatible with the neural transmission time, for the afferent (proprioceptive) feedback. In contrast, Granger causality analysis (applied to broadband signals) does not lead to reliable estimates of the delay times. Rather it only provides statistical approximations (by detecting accumulation points of delay estimates in an ensemble of tremor epochs), which correspond to the values obtained by the phase modelling approach. However, nonlinear Granger causality is even more sensitive for the detection of the efferent influence than the phase dynamics modelling. A detailed comparison between the theta band phase modelling analysis, the broadband nonlinear Granger causality analysis, and a spectral analysis shows that definitely the theta band LFP oscillations and possibly also the beta band LFP oscillations exert an efferent drive on the tremor.

Acknowledgments

We thank the EU network of excellence BioSim (LSHB-CT-20004-005137), BMBF (RUS 08/035) and the Russian Foundation for Basic Research (grant 07-02-00747).

References

[1] Jankovic J, McDermott M, Carter J, Gauthier S, Geotz C, Golbe L, Huber S, Koller W, Olanow C and Shoulson I 1990 Variable expression of Parkinson's disease: a base-line analysis of the datatop cohort. The Parkinson study group *Neurology* **40** 1529–34

[2] Marsden C D and Obeso J A 1994 The functions of the basal ganglia and the paradox of stereotaxic surgery in Parkinson's disease *Brain* **117** 877–8

[3] Obeso J A, Rodriguez M C and DeLong M R 1997 Basal ganglia pathophysiology: a critical review *Adv. Neurol.* **74** 3–18

[4] Brown P and Marsden C D 1998 What do the basal ganglia do? *Lancet* **351** 1801–4

[5] Deuschl G, Raethjen J, Baron R, Lindemann M, Wilms H and Krack P 2000 What do the basal ganglia do? The pathophysiology of parkinsonian tremor: a review *J. Neurol.* **247** (Suppl 5) 33–48

[6] Brown P 2003 Oscillatory nature of human basal ganglia activity: relationship to the pathophysiology of Parkinson's disease *Mov. Disord.* **18** 357–63

[7] Brown P and Williams D 2005 Basal ganglia local field potential activity: character and functional significance in the human *Clin. Neurophysiol.* **116** 2510–9

[8] Rivlin-Etzion M, Marmor O, Heimer G, Raz A, Nini A and Bergman H 2006 Basal ganglia oscillations and pathophysiology of movement disorders *Curr. Opin. Neurobiol.* **16** 629–37

[9] Deuschl G, Krack P, Lauk M and Timmer J 1996 Clinical neurophysiology of tremor *J. Clin. Neurophysiol.* **13** 110–21

[10] Zimmermann R, Deuschl G, Hornig A, Schulte-Mönting J, Fuchs G and Lucking C H 1994 Tremors in Parkinson's disease: symptom analysis and rating *Clin. Neuropharmacol.* **17** 303–14

[11] Koller W C, Vetere C B and Barter R 1989 Tremors in early Parkinson's disease *Clin. Neuropharmacol.* **12** 293–7

[12] Pollock L J and Davis L 1930 Muscle tone in parkinsonian states *Arch. Neurol. Psychiat.* **23** 303–9

[13] Putnam T J 1940 The operative treatment of diseases characterized by involuntary movements (tremor, athetosis) *Assoc. Res. Nerv. Ment. Dis.* **21** 666–96

[14] Cooper I 1969 Neurosurgical alleviation of intention tremor of multiple sclerosis and cerebellar disease *N. Engl. J. Med.* **263** 441–4

[15] Hassler R, Riechert T, Mundinger F, Umbach W and Gangelberger A 1960 Physiological observations in stereotactic operations in extrapyramidal motor disturbances *Brain* **83** 337–50

[16] Hassler R, Mundinger F and Riechert T 1979 *Stereotaxis in Parkinson Syndrome* (Berlin: Springer)

[17] Jung R 1941 Physiologische Untersuchungen über den Parkinsontremor und andere Zitterformen beim Menschen *Zsch. ges. Neurol. und. Psychiat.* **173** 263–332

[18] Lauk M, Koster B, Timmer J, Guschlbauer B, Deuschl G and Lucking C H 1999 Side to-side correlation of muscle activity in physiological and pathological human tremors *Clin. Neurophysiol.* **110** 1774–83

[19] Raethjen J, Lindemann M, Schmaljohann H, Wenzelburger R, Pfister G and Deuschl G 2000 Multiple oscillators are causing parkinsonian and essential tremor *Mov. Disord.* **15** 84–94

[20] Bergman H, Feingold A, Nini A, Raz A, Slovin H, Abeles M and Vaadia E 1998 Physiological aspects of information processing in the basal ganglia of normal and parkinsonian primates *Trends. Neurosci.* **21** 32–8

[21] Brown P, Oliviero A, Mazzone P, Insola A, Tonali P and Lazzaro V Di 2001 Dopamine dependency of oscillations between subthalamic nucleus and pallidum in Parkinson's disease *J. Neurosci.* **21** 1033–8

[22] Levy R, Ashby P, Hutchinson W D, Lang A E, Lozano A M and Dostrovsky J O 2002 Dependence of subthalamic nucleus oscillations on movement and dopamine in Parkinson's disease *Brain* **125** 1196–209

[23] Silberstein P *et al* 2003 There is a difference in patterning of globus pallidus local field potentials between pd and dystonia *Brain* **126** 2597–608

[24] Silberstein P, Oliviero A, Lazzaro V Di, Insola A, Mazzone P and Brown P 2005 Oscillatory pallidal local field potential activity inversely correlates with limb dyskinesias in Parkinson's disease *Exp. Neurol.* **194** 523–9

[25] Kühn A A, Kupsch A, Schneider G-H and Brown P 2006 Reduction in subthalamic 8–35 Hz oscillatory activity correlates with clinical improvement in Parkinson's disease *Eur. J. Neurosci.* **23** 1956–60

[26] Albe-Fessard D, Arfel G and Guiot G 1963 Activités électriques caractéristiques de quelques structures cérébrales chez l'homme *Ann. Chir.* **17** 1185–214

[27] Jasper H H and Bertrand G 1966 Thalamic units involved in somatic sensation and voluntary and involuntary movements in man *The Thalamus* ed D P Purpura and M D M Yahr (New York: Columbia University Press) pp 365–90

[28] Lenz F A, Tasker R R, Kwan H C, Schnider S, Kwong R, Murayama Y, Dostrovsky J O and Murphy J T 1988 Single unit analysis of the human ventral thalamic nuclear group: correlation of thalamic 'tremor cells' with the 3–6 Hz component of parkinsonian tremor *J. Neurosci.* **8** 754–64

[29] Lenz F A, Kwan H C, Dostrovsky J O, Tasker R R, Murphy J T and Lenz Y E 1990 Single unit analysis of the human ventral thalamic nuclear group: activity correlated with movement *Brain* **113** 1795–821

[30] Hutchison W D, Lozano A M, Tasker R R, Lang A E and Dostrovsky J O 1997 Identification and characterization of neurons with tremor-frequency activity in human globus pallidus *Exp. Brain. Res.* **113** 557–63

[31] Lozano A M, Lang A E and Hutchison W D 1998 Pallidotomy for tremor *Mov. Disord.* **13** 107–10

[32] Rodriguez M C, Guridi O J, Alvarez L, Mewes K, Macias R, Vitek J, DeLong M R and Obeso J A 1998 The subthalamic nucleus and tremor in Parkinson's disease *Mov. Disord.* **13** 111–8

[33] Hutchison W D, Allan R J, Opitz H, Levy R, Dostrovsky J O, Lang A E and Lozano A M 1998 Neurophysiological identification of the subthalamic nucleus in surgery for Parkinson's disease *Ann. Neurol.* **44** 622–8

[34] Krack P, Benazzouz A, Pollak P, Limousin P, Piallat B, Hoffmann D, Xie J and Benabid A L 1998 Treatment of tremor in Parkinson's disease by subthalamic nucleus stimulation *Mov. Disord.* **13** 907–14

[35] Amtage F, Henschel K, Schelter B, Vesperd J, Timmer J, Lücking C H and Hellwig B 2008 Tremor-correlated neuronal activity in the subthalamic nucleus of parkinsonian patients *Neurosci. Lett.* **442** 195–9

[36] Steigerwald F, Pötter M, Herzog J, Pinsker M, Kopper F, Mehdorn H, Deuschl G and Volkmann J 2008 Neuronal activity of the human subthalamic nucleus in the parkinsonian and nonparkinsonian state *J. Neurophysiol.* **100** 2515–24

[37] Moran A, Bergman H, Israel Z and Bar-Gad I 2008 Subthalamic nucleus functional organization revealed by parkinsonian neuronal oscillations and synchrony *Brain* **131** 3395–409

[38] Hurtado J M, Gray C M, Tamas L B and Sigvardt K A 1999 Dynamics of tremor-related oscillations in the human globus pallidus: a single case study *Proc. Natl Acad. Sci. USA* **96** 1674–9

[39] Levy R, Hutchison W D, Lozano A M and Dostrovsky J O 2000 High-frequency synchronization of neuronal activity in the subthalamic nucleus of parkinsonian patients with limb tremor *J. Neurosci.* **20** 7766–75

[40] Wang S Y, Aziz T Z, Stein J F and Liu X 2005 Time–frequency analysis of transient neuromuscular events: dynamic changes in activity of the subthalamic nucleus and forearm muscles related to the intermittent resting tremor *J. Neurosci. Methods* **145** 151–8

[41] Reck C, Florin E, Wojtecki L, Krause H, Groiss S, Voges J, Maarouf M, Sturm V, Schnitzler A and Timmermann L 2009 Characterisation of tremor-associated local field potentials in the subthalamic nucleus in Parkinson's disease *Eur. J. Neurosci.* **29** 599–612

[42] Schiff S J, So P, Chang T, Burke R E and Sauer T 1996 Detecting dynamical interdependence and generalized synchrony through mutual prediction in a neural ensemble *Phys. Rev.* E **54** 6708–24

[43] LeVanQuyen M, Martinerie J, Adam C and Varela F 1999 Nonlinear analyses of interictal EEG map the brain interdependences in human focal epilepsy *Physica* D **127** 250–66

[44] Arnhold J, Lehnertz K, Grassberger P and Elger C E 1999 A robust method for detecting interdependences: application to intracranially recorded EEG *Physica* D **134** 419–30

[45] Schreiber T 2000 Measuring information transfer *Phys. Rev. Lett.* **85** 461–4

[46] Hlavackova-Schindler K, Palus M, Vejmelka M and Bhattacharya J 2007 Causality detection based on information-theoretic approaches in time series analysis *Phys. Rep.* **441** 1–46

[47] Palus M and Vejmelka M 2007 Directionality of coupling from bivariate time series: How to avoid false causalities and missed connections *Phys. Rev.* E **75** 056211

[48] Romano M C, Thiel M, Kurths J and Grebogi C 2007 Estimation of the direction of the coupling by conditional probabilities of recurrence *Phys. Rev.* E **76** 036211

[49] Osterhage H, Mormann F, Wagner T and Lehnertz K 2007 Measuring the directionality of coupling: phase versus state space dynamics and application to EEG time series *Int. J. Neural Syst.* **17** 139–48

[50] Staniek M and Lehnertz K 2008 Symbolic transfer entropy *Phys. Rev. Lett.* **100** 158101

[51] Faes L, Porta A and Nollo G 2008 Mutual nonlinear prediction as a tool to evaluate coupling strength and directionality in bivariate time series: comparison among different strategies based on *k* nearest neighbors *Phys. Rev.* E **78** 026201

[52] Rosenblum M G and Pikovsky A S 2001 Detecting direction of coupling in interacting oscillator *Phys. Rev.* E **64** 045202

[53] Smirnov D A and Bezruchko B P 2003 Estimation of interaction strength and direction from short and noisy time series *Phys. Rev.* E **68** 046209

[54] Bahraminasab A, Ghasemi F, Stefanovska A, McClintock P V E and Kantz H 2008 Direction of coupling from phases of interacting oscillators: a permutation information approach *Phys. Rev. Lett.* **100** 084101

[55] Friston K J, Harrison L and Penny W 2003 Dynamic causal modelling *NeuroImage* **19** 1273–302

[56] Stephan K E, Kasper L, Harrison L M, Daunizeau J, den Ouden H E M, Breakspear M and Friston K J 2008 Nonlinear dynamic causal models for fMRI *NeuroImage* **42** 649–62

[57] Ancona N, Marinazzo D and Stramaglia S 2004 Radial basis function approach to nonlinear Granger causality of time series *Phys. Rev.* E **70** 056221

[58] Feldmann U and Bhattacharya J 2004 Predictability improvement as an asymmetrical measure of interdependence in bivariate time series *Int. J. Bifurcation Chaos* **14** 505–14

[59] Prusseit J and Lehnertz K 2008 Measuring interdependences in dissipative dynamical systems with estimated Fokker–Planck coefficients *Phys. Rev.* E **77** 041914

[60] Verdes P F 2005 Assessing causality from multivariate time series *Phys. Rev.* E **72** 026222

[61] Mokhov I I and Smirnov D A 2006 El nino southern oscillation drives North Atlantic oscillation as revealed with nonlinear techniques from climatic indices *Geophys. Res. Lett.* **33** L0378 doi:10.1029/2005GL024557

[62] Mosedale T J, Stephenson D B, Collins M and Mills T C 2006 Granger causality of coupled climate processes: ocean feedback on the North Atlantic oscillation *J. Climate.* **19** 1182–94

[63] Rosenblum M G, Bezerianos L C L A, Patzak A and Mrowka R 2002 Identification of coupling direction: application to cardiorespiratory interaction *Phys. Rev.* E **65** 041909

[64] Palus M and Stefanovska A 2003 Direction of coupling from phases of interacting oscillators: an information-theoretic approach *Phys. Rev.* E **67** 055201

[65] Prokhorov M D, Ponomarenko V I, Gridnev V I, Bodrov M B and Bespyatov A B 2003 Synchronization between main rhythmic processes in the human cardiovascular system *Phys. Rev.* E **68** 041913

[66] Luchinsky D G, Millonas M M, Smelyanskiy V N, Pershakova A, Stefanovska A and McClintock P V 2005 Nonlinear statistical modeling and model discovery for cardiorespiratory data *Phys. Rev.* E **72** 021905

[67] Pereda E, Quian Quiroga R and Bhattacharya J 2005 Nonlinear multivariate analysis of neurophysiological signals *Prog. Neurobiol.* **77** 1–37

[68] Brea J, Russell D F and Neiman A B 2006 Measuring direction in the coupling of biological oscillators: a case study for electroreceptors of paddlefish *Chaos* **16** 026111

[69] Granger C W I 1969 Investigating causal relations by econometric models and cross-spectral methods *Econometrica* **37** 424–38

[70] Smirnov D A and Andrzejak R G 2005 Detection of weak directional coupling: phase dynamics approach versus state space approach *Phys. Rev.* E **71** 036207

[71] Smirnov D A, Schelter B, Winterhalder M and Timmer J 2007 Revealing direction of coupling between neuronal oscillators from time series: phase dynamics modeling versus partial directed coherence *Chaos* **17** 013111

[72] Smirnov D A, Barnikol U B, Barnikol T T, Bezruchko B P, Hauptmann C, Buehrle C, Maarouf M, Sturm V, Freund H-J and Tass P A 2008 The generation of parkinsonian tremor as revealed by directional coupling analysis *Europhys. Lett.* **83** 20003

[73] Benabid A L, Pollak P, Louveau A, Henry S and de Rougemont J 1987 Combined (thalamotomy and stimulation) stereotactic surgery of the VIM thalamic nucleus for bilateral Parkinson's disease *Appl. Neurophysiol.* **50** 344–6

[74] Treuer H, Klein D, Maarouf M, Lehrke R, Voges J and Sturm V 2005 Accuracy and conformity of stereotactically guided interstitial brain tumour therapy using I-125 seeds *Radiother. Oncol.* **77** 202–9

[75] Eichler M 2006 Graphical modelling of dynamic relationships in multivariate time series *Handbook of Time Series Analysis* ed M Winterhalder, B Schelter and J Timmer (Berlin: Wiley-VCH) pp 335–67

[76] Winterhalder M, Schelter B, Hesse W, Schwab K, Leistritz L, Klan D, Bauer R, J Timmer J and Witte H 2005 Comparison of linear signal processing techniques to infer directed interactions in multivariate neural systems *Signal Process.* **85** 2137–60

[77] Schreiber T and Schmitz A 2000 Surrogate time series *Physica* D **142** 346–82

[78] Priori A, Ardolino G, Marceglia S, Mrakic-Sposta S, Locatelli M, Tammab F, Rossi L and Foffani G 2006 Low-frequency subthalamic oscillations increase after deep brain stimulation in Parkinson's disease *Brain. Res. Bull.* **71** 149–54

[79] Rybski D, Havlin S and Bunde A 2003 Phase synchronization in temperature and precipitation records *Physica* A **320** 601–10

[80] Gozolchiani A, Moshela S, Hausdorff J M, Simon E, Kurths J and Havlin S 2006 Decaying of phase synchronization in parkinsonian tremor *Physica* A **366** 552–60

[81] Gabor D 1946 Theory of communication *J. Inst. Elect. Eng. (London)* **93** 429–59

[82] Rosenblum M G, Pikovsky A S, Kurths J, Schaefer C and Tass P A 2001 Phase synchronization: from theory to data analysis *Neuro Informatics. Handbook of Biological Physics* ed F Moss and S Gielen (New York: Elsevier) pp 279–321

[83] Cimponeriu L, Rosenblum M and Pikovsky A 2004 Estimation of delay in coupling from time series *Phys. Rev.* E **70** 046213

[84] Smirnov D A, Karpeev I A and Bezruchko B P 2007 Detection of coupling between oscillators from their short time series: condition of applicability of the method of phase dynamics modeling *Tech. Phys. Lett.* **33** 147–50

[85] Tass P, Rosenblum M G, Weule J, Kurths J, Pikovsky A, Volkmann J, Schnitzler A and Freund H-J 1998 Detection of *n:m* phase locking from noisy data: application to magnetoencephalography *Phys. Rev. Lett.* **81** 3291–4

[86] Tass P A, Fieseler T, Dammers J, Dolan K, Morosan P, Majtanik M, Boers F, Muren A, Zilles K and Fink G R 2003 Synchronization tomography: a method for three-dimensional localization of phase synchronized neuronal populations in the human brain using magnetoencephalography *Phys. Rev. Lett.* **90** 088101

[87] Dietz V 2003 Spinal cord pattern generators for locomotion *Clin. Neurophysiol.* **114** 1379–89

[88] Klostermann F, Vesper J and Curio G 2003 Identification of target areas for deep brain stimulation in human basal ganglia substructures based on median nerve sensory evoked potential criteria *J. Neurol. Neurosurg. Psychiatry* **74** 1031–5

[89] Stilles R and Pozos R 1976 A mechanical-reflex oscillator hypothesis for parkinsonian hand tremor *J. Appl. Physiol.* **40** 990–8

[90] Fogelson N, Williams D, Tijssen M, van Bruggen G, Speelman H and Brown P 2006 Different functional loops between cerebral cortex and the subthalamic area in Parkinson's disease *Cereb. Cortex.* **16** 64–75

[91] Lalo E, Thobois S, Sharott A, Polo G, Mertens P, Pogosyan A and Brown P 2008 Patterns of bidirectional communication between cortex and basal ganglia during movement in patients with Parkinson's disease *J. Neurosci.* **28** 3008–16

[92] von Holst E 1939 Die relative Koordination als Phänomen und als Methode zentralnervöser Funktionsanalysen *Erg. Physiol.* **42** 228–306

[93] Kelso J A S 1995 *Dynamic Patterns: The Self-Organization of Brain and Behavior* (Cambridge: MIT Press)

[94] Haken H 1996 *Principles of Brain Functioning. A Synergetic Approach to Brain Activity, Behavior and Cognition* (Berlin: Springer)

[95] Levy R, Hutchison W D, Lozano A M and Dostrovsky J O 2002 Synchronized neuronal discharge in the basal ganglia of parkinsonian patients is limited to oscillatory activity *J. Neurosci.* **22** 2855–61

[96] Weinberger M, Mahant N, Hutchison W D, Lozano A M, Moro E, Hodaie M, Lang A E and Dostrovsky J O 2006 Beta oscillatory activity in the subthalamic nucleus and its relation to dopaminergic response in Parkinson's disease *J. Neurophysiol.* **96** 3248–56

[97] Cassidy M, Mazzone P, Oliviero A, Insola A, Tonali P, Di Lazzaro V and Brown P 2002 Movement-related changes in synchronisation in the human basal ganglia *Brain* **125** 1235–46

[98] Wang S, Chen Y, Ding M, Feng J, Stein J F, Aziz T Z and Liu X J 2007 Revealing the dynamic causal interdependence between neural and muscular signals in parkinsonian tremor *J. Franklin Inst.* **344** 180–95

[99] Florina E, Reck C, Burghaus L, Lehrke R, Gross J, Sturm V, Fink G R and Timmermann L 2008 Ten hertz thalamus stimulation increases tremor activity in the subthalamic nucleus in a patient with Parkinson's disease *Clin. Neurophysiol.* **119** 2098–103

[100] Lenz F A, Tasker R R, Kwan H C, Schnider S, Kwong R and Murphy J T 1985 Cross-correlation analysis of thalamic neurons and EMG activity in parkinsonian tremor *Appl. Neurophysiol.* **48** 305–8

[101] Lenz F A, Schnider S, Tasker R R, Kwong R, Kwan H C, Dostrovsky J O and Murphy J T 1987 The role of feedback in the tremor frequency activity of tremor cells in the ventral nuclear group of human thalamus *Acta Neurochir. Suppl.* **39** 54–6

[102] Lenz F A, Vitek J L and DeLong M R 1993 Role of the thalamus in parkinsonian tremor: evidence from studies in patients and primate models *Stereotact. Funct. Neurosurg.* **60** 94–103

[103] Lenz F A, Kwan H C, Martin R L, Tasker R R, Dostrovsky J O and Lenz Y E 1994 Single unit analysis of the human ventral thalamic nuclear group. Tremor-related activity in functionally identified cells *Brain* **117** 531–43

[104] Zirh T A, Lenz F A, Reich S G and Dougherty P M 1998 Patterns of bursting occurring in thalamic cells during parkinsonian tremor *Neuroscience* **83** 107–21

[105] Hassler R 1959 Anatomy of the thalamus *Introduction to Stereotaxis with an Atlas of the Human Brain* ed G Schaltenbrand and P Bailey (Stuttgart: Thieme) pp 230–90

[106] Hirai T and Jones E G 1989 A new parcellation of the human thalamus on the basis of histochemical staining *Brain Res. Rev.* **14** 1–34

[107] Llinas R 1984 Rebound excitation as the physiological basis for tremor: a biophysical study of the oscillatory properties of mammalian central neurons *in vitro Movement Disorders, Tremor* ed L J Findley and R Capildeo (London: Macmillan) pp 339–51

[108] Tatton W G and Lee R G 1975 Evidence for abnormal long-loop reflexes in rigid parkinsonian patients *Brain Res.* **100** 671–6

[109] Stein R B and Oguztoreli M N 1976 Tremor and other oscillations in neuromuscular systems *Biol. Cybern.* **22** 147–57

[110] Krack P, Benazzouz A, Pollak P, Limousin P, Piallat B, Hoffmann D, Xie J and Benabid A L 1998 Treatment of

tremor in Parkinson's disease by subthalamic nucleus stimulation *Mov. Disord.* **13** 907–14

[111] Rodriguez-Oroz M C, Rodriguez M, Guridi J, Mewes K, Chockkman V, Vitek J, DeLong M R and Obeso J A 2001 The subthalamic nucleus in Parkinson's disease: somatotopic organization and physiological characteristics *Brain* **124** 1777–90

[112] Plenz D and Kital S T 1999 A basal ganglia pacemaker formed by the subthalamic nucleus and external globus pallidus *Nature* **400** 677–82

[113] Mandir A S, Rowland L H, Dougherty P M and Lenz F A 1997 Microelectrode recording and stimulation techniques during stereotactic procedures in the thalamus and pallidum *The Basal Ganglia and New Surgical Approaches for Parkinson's Disease* ed J A Obeso, M R DeLong, C Ohye and C D Marsden (Philadelphia: Lippincott-Raven) pp 159–65

[114] Filion M, Tremblay L, Matsumura M and Richard H 1994 Dynamic focusing of informational convergence in basal ganglia *Rev. Neurol. (Paris)* **150** 627–33

[115] Nini A, Feingold A, Slovin H and Bergman H 1995 Neurons in the globus pallidus do not show correlated activity in the normal monkey, but phase-locked oscillations appear in the MPTP model of parkinsonism *J. Neurophysiol.* **74** 1800–5

[116] Vitek J L and Giroux M 2000 Physiology of hypokinetic and hyperkinetic movement disorders: model for dyskinesia *Ann. Neurol.* **47** S131–40

[117] Tass P A 1999 *Phase Resetting in Medicine and Biology. Stochastic Modelling and Data Analysis* (Heidelberg: Springer)

[118] Tass P A 2003 A model of desynchronizing deep brain stimulation with a demand-controlled coordinated reset of neural subpopulations *Biol. Cybern.* **89** 81–8

[119] Benabid A L, Pollak P, Gervason C, Hoffmann D, Gao D M, Hommel M, Perret J E and De Rougemont J 1991 Long-term suppression of tremor by chronic stimulation of the ventral intermediate thalamic nucleus *The Lancet.* **337** 403–6

[120] Benabid A L, Benazzous A and Pollak P 2002 Mechanisms of deep brain stimulation *Mov. Disord.* **17** 73–4

[121] Benabid A L, Wallace B, Mitrofanis J, Xia R, Piallat B, Chabardes S and Berger F 2005 A putative generalized model of the effects and mechanism of action of high frequency electrical stimulation of the central nervous system *Acta Neurol. Belg.* **105** 149–57